PCCP

Accepted Manuscript

ROYAL SOCIETY OF CHEMISTRY

www.rsc.org/pccp

Role of oxygen impurity on the mechanical stability and atomic cohesion of Ta_3N_5 semiconductor photocatalyst

Jiajia Wang, Jianyong Feng, Li Zhang, Zhaosheng Li* and Zhigang Zou*

National Laboratory of Solid State Microstructures, Department of Physics, Ecomaterials and Renewable Energy Research Center (ERERC), and College of Engineering and Applied Sciences, Nanjing University, 22 Hankou Road, Nanjing 210093, People's Republic of China.

* Corresponding Authors: Tel: +86-25-83686630, Fax: +86-25-83686632, E-mail: zsli@nju.edu.cn (Z. S. Li) or zgzou@nju.edu.cn (Z. G. Zou)

ABSTRACT: Oxygen is a natural impurity in the Ta_3N_5 semiconductor photocatalyst and very difficult to be completely eliminated in different growth conditions. In this study, density functional theory calculations are performed to unravel the cause of natural existence of oxygen impurity in Ta_3N_5 from the perspectives of mechanical stability and atomic cohesion. The elastic properties calculations show that the oxygen impurity in Ta_3N_5 is able to remedy the weakened mechanical stability induced by the nitrogen vacancy in Ta_3N_5. The atomic cohesion calculations show that the oxygen impurity in Ta_3N_5 enlarges the valence band width of Ta_3N_5, suggesting that the oxygen impurity is able to strengthen the atomic cohesion of Ta_3N_5. Based on our calculation results, we propose that the charge-compensation-codoping is a promising strategy to improve the water splitting ability of Ta_3N_5 and simultaneously maintain the mechanical stability and enhanced atomic cohesion of Ta_3N_5.

1. Introduction

Solar hydrogen production *via* photocatalytic or photoelectrochemical water splitting is a promising strategy to ease current energy shortage and environmental crisis, because it supplies an environmentally approach for splitting water into H_2 and O_2 under irradiation of solar light[1-3]. One key issue for realizing this application is to develop suitable semiconductor photocatalysts which can absorb more abundant visible light. Recently, tantalum nitride (Ta_3N_5) as one semiconductor photocatalyst has attracted great interest because of its excellent performance of water splitting in the visible light region[4-6]. Due to the smaller band gap (about 2.1 eV) and appropriate band edges positions, the theoretical maximum solar-to-hydrogen efficiency of Ta_3N_5 is as high as 15.9%[7].

For metal oxides and nitrides, the most common intrinsic defects are anion vacancies, which play critical roles in various applications. In Ta_3N_5, besides the nitrogen vacancy (V_N), the other important defect is the oxygen impurity (O_N). Note that, although the nominal constitutional elements of Ta_3N_5 are only composed of N and Ta, experiments reveal that the real synthesized Ta_3N_5 samples consist of considerable amounts of the O_N impurities[8, 9]. One proper O_N impurity source comes from the tantalum oxides (Ta_2O_5) because Ta_3N_5 is usually synthesized by heating Ta_2O_5 under environment of flowing ammonia gas. Moreover, it is very difficult to thoroughly eliminate the O_N impurity in Ta_3N_5, even though the Ta_3N_5 samples are heated with higher temperature and longer time[8, 9]. Therefore, the real Ta_3N_5 samples should be reasonably denoted as the O-doped Ta_3N_5. Theoretical calculations also revealed that formation energy of O_N impurity was smaller than that of the V_N defect in Ta_3N_5[10]. In addition, we recently made a theoretical study of the pure Ta_3N_5 (100) surface and Ta_3N_5 (100) surfaces with O_N impurity and V_N defect[11]. Surface energies indicated that the order of surface stability of different surfaces was Ta_3N_5

(100) surface with O_N impurity > pure Ta_3N_5 (100) surface > Ta_3N_5 (100) surface with V_N defect, suggesting that the V_N defect did not facilitate surface stability while the O_N impurity was able to help stabilize the Ta_3N_5 (100) surface.

Formation energy and surface energy results validate the rationality of the experimental observation of O_N impurity in Ta_3N_5. However, both formation energy and surface energy are merely thermodynamic properties, which are insufficient to provide an in-depth understanding of the role of O_N impurity in Ta_3N_5. In this study, density functional theory (DFT) calculations are performed to compare O_N impurity and V_N defect from the perspectives of mechanical stability and atomic cohesion, which correspond to the macroscopic and microscopic properties, respectively. To evaluate the effects of O_N impurity and V_N defect on the mechanical stability of Ta_3N_5, typical mechanical parameters such as elastic constants, bulk modulus and shear modulus are calculated. To evaluate the effects of O_N impurity and V_N defect on the atomic cohesion of Ta_3N_5, the valence band width (VBW) is calculated in this study. The VBW of a semiconductor is a useful property to measure the atomic cohesion of a semiconductor. More details of the correlation between atomic cohesion and VBW will be discussed in next section. By the comparisons between O_N impurity and V_N defect, we can unravel the cause of natural existence of O_N impurity in Ta_3N_5. This study is expected to be useful to provide indications for further theoretical and experimental investigations of Ta_3N_5 semiconductor photocatalyst.

2. Computational details

In this study, mechanical stability and atomic cohesion are reflected by elastic constants and VBW, respectively. With the development of current DFT calculations, elastic constants are relatively easier calculated. The orthorhombic Ta_3N_5 (space group:

Cmcm) has nine independent elastic constants (c_{11}, c_{22}, c_{33}, c_{44}, c_{55}, c_{66}, c_{12}, c_{13}, c_{23}), and its elastic constants are calculated using the method proposed by Ravindran[12], et al. The bulk modulus (B) and shear modulus (G) are derived from the Voigt-Reuss-Hill approximation[13]. The Young's modulus (E) is calculated from B and G. More details of the elastic constants calculations can be found in the support information.

The calculation of VBW should be paid more attentions. Recently, Ramprasad[14], et al. proposed that VBW of a semiconductor is a useful property to measure the *atomic cohesive interaction* between the respective atoms within the semiconductor. The bigger the VBW is, the greater the atomic cohesion is, and thus the larger the resistance to form defects in the semiconductor will be. Since the VBW is the measure of atomic cohesion of a semiconductor, the change of VBW induced by exterior influence can be adopted to evaluate whether such exterior influence is easily accommodated or not by the semiconductor. For example, in a doped semiconductor, if the introduction of one doped element enlarges (or reduces) the VBW of the semiconductor, the atomic cohesion of the element semiconductor is strengthened (or weakened), suggesting that this doped element is easily (or difficultly) formed in this semiconductor. In this study, we will compare the VBWs of Ta_3N_5 with O_N impurity and V_N defect to reveal effects of O_N impurity and V_N defect on the atomic cohesion of Ta_3N_5.

In Ramprasad, et al.'s work[14], the relationship between atomic cohesion and VBW is derived from the linear correlation of defect formation energies with VBWs. Typical semiconductors such as Si, Ge, ZnO and ZrO_2 are used as parent materials to validate this relationship in their work. However, whether the atomic cohesion of Ta_3N_5 can also be measured by the VBW of Ta_3N_5 needs to be validated. Then, similar to the calculation scheme in Ramprasad, et al.'s work, we exploit the availability of the (α, ω) parameter

space of the Heyd-Scuseria-Ernzerhof (HSE[15]) "family" of the hybrid functional method. For the HSE, the exchange-correlation functional is built from a semilocal Perdew-Burke-Ernzerhof (PBE[16]) functional. The parameter α represents the fraction of the semilocal PBE exchange interaction replaced by a screened nonlocal functional, and ω is the inverse screening length[17]. By variations of α and ω parameters, the VBWs and the defect formation energies of the pure and defective Ta_3N_5 can be modulated, respectively. We consider five specific functionals in the (α, ω) parameter space: PBE, PBE0, HSE, $HSE_{>\alpha}$ and $HSE_{>\omega}$. The PBE and PBE0 refer to the (0.25, ∞) and (0.25, 0) hybrid functionals, respectively. The HSE refers to the (0.25, 0.2 $Å^{-1}$) HSE06 functional[17], while the $HSE_{>\alpha}$ and $HSE_{>\omega}$ correspond to (0.5, 0.2 $Å^{-1}$) and (0.25, 0.4 $Å^{-1}$), respectively.

We construct a conventional Ta_3N_5 cell which contains 20N and 12Ta atoms [Fig. 1(a)]. In Ta_3N_5, the Ta atom is coordinated with six neighboring N atoms, while N atoms are coordinated with three or four Ta atoms. Since both experiments[9] and theoretical calculations[11] have proved that the 3-coordinated N atom is easier substituted by the O atom, only the 3-coordinated N atom is removed and substituted by one O atom to build the Ta_3N_5 with V_N (denoted as $Ta_3N_5+V_N$) and O-doped Ta_3N_5 (denoted as $Ta_3N_5+O_N$), respectively. The O doping concentration in this Ta_3N_5 cell is 5%, which is very close to the about 5% O doping concentration in experiments[8, 9]. The formation energy of the O_N impurity in Ta_3N_5 in the neutral charge state is given by[18]:

$$E^f(O_N) = E^t(O_N) - E^t(pure) + \mu_N - \mu_O \quad (1)$$

where $E^t(O_N)$ and $E^t(pure)$ are total energies of the cells with and without the O_N impurity, respectively. μ_O and μ_N are the chemical potentials of O and N and simply using half the energy per O_2 molecule and N_2 molecule, respectively. The formation energy of the

V_N defect in the neutral charge state is the same as that of O_N impurity without the μ_O term in Eq. (1).

The VBW is defined by the energy separation of valence band maximum (VBM) and valence band minimum (VBm) in the valence band (E_{VBW}=E_{VBM}-E_{VBm}). The VBM of a semiconductor is easily understood. The VBm of one semiconductor is a point at which the energy is the minimum in the whole valence band. To find the VBM and VBm of Ta_3N_5, some high symmetry *k*-points in the Brillouin zone of Ta_3N_5 are selected and shown in Fig. 1(b). Based on this *k*-points path, the band structure of the pure conventional bulk Ta_3N_5 is calculated and shown in Fig. 1(c). As can be seen, the valence band of Ta_3N_5 is composed of 60 bands. The VBM at the Γ point is not degenerate state while the VBm at the T point is four-fold degeneracy, leading to 15 degenerate states at the T point. Since the VBM and VBm of the pure Ta_3N_5 are locating at the Γ and T high symmetry points, respectively, the VBW of Ta_3N_5 is calculated by the energy separation of the Γ and T points.

Both elastic constants and VBW calculations are performed using the VASP[19] with the projector augmented wave (PAW[20]) methodology. The Γ-centered 4×2×2 *k*-point meshes and a plane wave energy cutoff of 450 eV are used. Geometry optimizations are performed until the residual forces on each ion converged to be smaller than 0.01 eV/Å. Similar to the calculation scheme in Ramprasad, et al.'s work[14], geometry optimizations for the VBW calculations are performed at the PBE level of theory, and the PBE optimized geometry is used in other hybrid functional calculations.

3. Results and discussion

3.1 Mechanical stability

The calculated elastic constants, bulk modulus *B*, shear modulus *G*, and Young's modulus *E* of the pure Ta_3N_5, Ta_3N_5+V_N and Ta_3N_5+O_N under ambient pressure are listed in Table 1. Due to the lack of experimental elastic properties of Ta_3N_5, it is difficult to make a comparison between our calculated results and experimental results. Our elastic constants calculation method is the energy-strain method[12]. To ensure the reliability of this method, we calculate elastic constants of another tantalum nitride Ta_2N_3 which is also the orthorhombic crystal structure. Our calculated elastic constants of Ta_2N_3 (see Table S1 of the support information) are in good agreement with other theoretical results[21]. Moreover, our calculated *B* of Ta_2N_3 (327 GPa) is also in good agreement with the experimental value[22] (319 GPa), suggesting that the energy-strain method for the elastic constants calculation is theoretically reliable.

For the orthorhombic crystal structure to be mechanically stable, its elastic constants should satisfy the following stability criteria[23]:

$$c_{11} > 0, c_{22} > 0, c_{33} > 0, c_{44} > 0, c_{55} > 0,$$

$$c_{66} > 0, c_{11} + c_{22} + c_{33} + 2(c_{12} + c_{13} + c_{23}) > 0, \quad (2)$$

$$c_{11} + c_{22} - 2c_{12} > 0, c_{11} + c_{33} - 2c_{13} > 0, c_{22} + c_{33} - 2c_{23} > 0.$$

As can be seen in Table 1, elastic constants of Ta_3N_5+V_N and Ta_3N_5+O_N satisfy above stability criteria, suggesting that the O_N impurity and V_N defect do not affect the mechanical stability of Ta_3N_5. However, detailed analysis of all elastic properties reveals that, elastic constants, *B*, *G* and *E* of Ta_3N_5+V_N are smaller than that of the pure Ta_3N_5, suggesting that formation of V_N defect in Ta_3N_5 weakens the mechanical stability of Ta_3N_5. When the O_N impurity formed in Ta_3N_5, the elastic constants, *B*, *G* and *E* of Ta_3N_5+O_N are larger than

that of Ta_3N_5+V_N, and very close to that of the pure Ta_3N_5. This means that formation of O_N impurity in Ta_3N_5 is able to remedy the weakened mechanical stability of Ta_3N_5+V_N.

Actually, the O_N impurity has also been found in other tantalum nitrides such as Ta_2N_3[21] and Ta_5N_6[24], in which the O_N impurity has also been proved to help make the structure mechanically stable by significantly increasing the shear modulus. In Ta_2N_3, the O_N impurity is especially important because the orthorhombic structure of Ta_2N_3 is mechanically unstable without the O_N impurity. It is not appropriate to state that all tantalum nitrides include the O_N impurities, but above experiments, as well as our calculated results of Ta_3N_5, clearly reveal that the O_N impurity plays a critical role in the structural stabilization of tantalum nitrides. Mechanical stability is a macroscopic property and usually correlated with the microscopic properties. In next section, we will further investigate the O_N impurity and V_N defect in Ta_3N_5 from the viewpoint of atomic cohesion.

3.2 Atomic cohesion

As we have discussed in the computational details section, in order to use VBW to evaluate the atomic cohesion of Ta_3N_5, we firstly need to validate whether the linear correlation of defect formation energies with VBW is also applied for Ta_3N_5. Fig. 2 shows the dependence of formation energies of the O_N impurity and V_N defect on the VBWs of the pure Ta_3N_5. It is seen that, for both the O_N impurity and V_N defect, the formation energies increase in the order: PBE, $HSE_{>\omega}$, HSE, PBE0 and $HSE_{>\alpha}$. This order may be ascribed to the fact that HSE with a finite ω is an interpolation between the PBE and PBE0. The increasing order of formation energies with the monotonic variation of ω value is also found in other theoretical work[17]. Moreover, the correlation of formation energies of the O_N impurity and V_N defect with VBWs are linear, suggesting that our calculated results of

Ta_3N_5 reproduce the findings in Ramprasad, et al.'s work[14]. In other words, the strength of atomic cohesion of Ta_3N_5 can also be measured by the VBW of Ta_3N_5. Then, by calculating the change of VBW when the O_N impurity and V_N defect formed in Ta_3N_5, we can evaluate the effects of O_N impurity and V_N defect on the atomic cohesion of Ta_3N_5.

Fig. 3(a) shows the dependence of VBWs on different hybrid functionals for the pure Ta_3N_5, Ta_3N_5+O_N and Ta_3N_5+V_N. As can be seen, regardless of the hybrid functional, the VBWs of the Ta_3N_5+O_N and Ta_3N_5+V_N are bigger and smaller than that of the pure Ta_3N_5, respectively. According to above discussion, this means that the O_N impurity and V_N defect are able to strengthen and weaken the atomic cohesion of Ta_3N_5, respectively. This also provides a possible explanation for the role of O_N impurity and V_N defect on the mechanical stability of Ta_3N_5. We also calculate the cohesive energies of the pure Ta_3N_5, Ta_3N_5+O_N and Ta_3N_5+V_N to quantitatively evaluate the strength of atomic cohesion. The cohesive energy is defined as[25]:

$$E_{cohesive} = \sum n_i E_i - E_{bulk} \quad (3)$$

where E_{bulk} is the total energy of the pure Ta_3N_5 or defective Ta_3N_5, n_i and E_i (i=N, O, Ta) are the number and energy of each constitutional atom, respectively. According to this definition, a more positive cohesive energy corresponds to a stronger atomic cohesion. The cohesive energies in Fig. 3(b) show that, for each exchange-correlation functional, the order of cohesive energies among Ta_3N_5, Ta_3N_5+V_N and Ta_3N_5+O_N is the same as that of the VBWs in Fig. 3(a), confirming that the O_N impurity and V_N defect are able to strengthen and weaken the atomic cohesion of Ta_3N_5, respectively.

To aid the in-depth understanding of the discrepancies in VBWs among the pure Ta_3N_5, Ta_3N_5+O_N and Ta_3N_5+V_N, their detailed valence band structures are studied and

shown in Fig. 4(a) to 4(c), respectively. For the pure Ta_3N_5, the VBM at the Γ point is not degenerate state while the VBm at the T point is four-fold degeneracy. When the O_N impurity and V_N defect formed in Ta_3N_5, the four-fold degeneracy at the T point is broken, inducing enlargement and reduction of the VBWs in Ta_3N_5+O_N and Ta_3N_5+V_N, respectively. We further calculate the charge density difference of the four lowest energy bands in the valence band between the pure Ta_3N_5 and Ta_3N_5+O_N [Fig. 4(d)], and that between the pure Ta_3N_5 and Ta_3N_5+V_N [Fig. 4(e)]. Compared with the V_N defect which depletes charge from the Ta-N bond, the O_N impurity induces charge accumulation along the Ta-O bond. Therefore, although both the O_N impurity and V_N defect are able to breach the four-fold degeneracy at the T point, the reinforced Ta-O bond strengthens the atomic cohesion of Ta_3N_5 and leads the atomic structure of Ta_3N_5+O_N to a lower energy level.

Above results clearly reveal that the O_N impurity facilitates the mechanical stability and atomic cohesion of Ta_3N_5. However, our recent work reveals that the O_N impurity should be as less as possible in Ta_3N_5 because the O_N impurity saturates surface dangling bonds and thus lowering the water splitting ability of the Ta_3N_5 (100) surface[11]. To reveal the real effects of O_N impurity doping on the water splitting ability of Ta_3N_5, the more accurate HSE calculations are carried out in this study. Firstly, we investigate the band gap calculated by different functionals. The band gap calculated by PBE, $HSE_{>\omega}$, HSE, PBE0 and $HSE_{>\alpha}$ are 1.25, 1.83, 2.21, 2.91 and 3.34 eV, respectively. It is seen that, due to the well-known band gap underestimation of the PBE functional, the band gap calculated by PBE is smaller than the experimental value of Ta_3N_5. For the hybrid functionals, the 2.21 eV band gap calculated by HSE (also known as HSE06[17], α=0.25, ω=0.2 $Å^{-1}$) is in good agreement with the experimental value (about 2.1 eV). To our knowledge, the HSE functional has been successfully used in the band gap and defect states calculations for

many semiconductors. For example, with the HSE functional, the defect states positions induced by the oxygen vacancy in TiO_2 can be correctly presented in the band gap[26].

Secondly, we calculate density of states (DOS) of Ta_3N_5, Ta_3N_5+V_N and Ta_3N_5+O_N to investigate the effects of O_N impurity doping and V_N defect doping on the electronic structures of Ta_3N_5. Since only HSE is able to reproduce the experimental band gap of Ta_3N_5, the DOS calculations are only based on the HSE functional. However, to make a comparison between the PBE and HSE functioanls, the DOS of Ta_3N_5, Ta_3N_5+V_N and Ta_3N_5+O_N at the PBE level are firstly calculated and shown in Fig. 5(a), 5(b) and 5(c) respectively. Note that, to correctly evaluate the relative band shift, the horizontal axes of Ta_3N_5+V_N and Ta_3N_5+O_N are aligned with that of pure Ta_3N_5 by the electrostatic potential calculations. It is seen that, there is an in-gap defect state in the band gap of Ta_3N_5+V_N. This defect state is close to the conduction band minimum (CBM). Further analysis reveals that the VBM and CBM of Ta_3N_5+V_N shift left compared with that of the pure Ta_3N_5. Such left shift of VBM and CBM is also found in the DOS of Ta_3N_5+O_N. The DOS of Ta_3N_5, Ta_3N_5+V_N and Ta_3N_5+O_N calculated by HSE are shown in Fig. 5(d), 5(e) and 5(f) respectively. The horizontal axes of Ta_3N_5+V_N and Ta_3N_5+O_N are also aligned with that of pure Ta_3N_5 by the electrostatic potential calculations. It is seen that, in Ta_3N_5+V_N, a defect state lies near the center of the band gap, confirming the results in Fig. 5(b) calculated at the PBE level. Since HSE is able to reproduce the experimental band gap of Ta_3N_5, the defect state position in Fig. 5(e) is more reliable. The left shift of VBM and CBM in Ta_3N_5+V_N and Ta_3N_5+O_N are also found in Fig. 5(e) and 5(f), reconfirming results calculate by the PBE functional.

Since the CBM position of one semiconductor reflects its reduction ability to split water into H_2, the left shift of CBM in Ta_3N_5+O_N and Ta_3N_5+V_N suggests that the O_N

impurity and V_N defect are possible sources of the poor H_2 evolution of Ta_3N_5. Due to the large concentrations of O_N impurities in Ta_3N_5[8, 9], the O_N impurity plays a more important role in the photocatalytic water splitting of Ta_3N_5. However, enhancing the water splitting ability of Ta_3N_5 by eliminating O_N impurity is not feasible because O_N impurity facilitates the mechanical stability and atomic cohesion of Ta_3N_5. Considering that the O_N impurity is one electron donor in Ta_3N_5, we propose that the charge-compensation-codoping is a promising strategy to improve the water splitting ability of Ta_3N_5 and simultaneously maintain the enhanced atomic cohesion induced by the O_N impurity. Elements which are able to donate holes can be codoped with the O_N impurity to make the charge compensation and thus weakening the effects of O_N impurity on the water splitting ability of Ta_3N_5. The Cr-La codoped $SrTiO_3$, in which Cr and La substitute for Ti and Sr, respectively, is exactly a successful example of such charge-compensation-codoping strategy[27].

4. Conclusion

In summary, based on the hybrid-DFT calculations, we investigate the role of O_N impurity on the mechanical stability and atomic cohesion of Ta_3N_5 semiconductor photocatalyst. The study of elastic properties of the pure Ta_3N_5, Ta_3N_5+V_N and Ta_3N_5+O_N reveal that, the V_N defect weakens the mechanical stability of Ta_3N_5 while the O_N impurity is able to remedy the weakened mechanical stability of Ta_3N_5+V_N. Based on the relationship between atomic cohesion and valance band width of a semiconductor, we investigate the effects of O_N impurity on the atomic cohesion of Ta_3N_5. We found that the introduction of O_N impurity into Ta_3N_5 enlarges the valence band width of Ta_3N_5, suggesting that the O_N impurity is able to strengthen the atomic cohesive interaction within Ta_3N_5. This study unravels the cause of natural existence of O_N impurity in Ta_3N_5 from

macroscopic and microscopic perspectives and, more importantly, provides useful indications for further investigations of Ta_3N_5.

Acknowledgements

The authors thank financial support from National Basic Research Program of China (973 Program, 2013CB632404), a Project Funded by the Priority Academic Program Development of Jiangsu Higher Education Institutions, New Century Excellent Talents in University (NCET-12-0268), and the National Natural Science Foundation of China (Nos. 51272101 and 51272102), and the Jiangsu Provincial Natural Science Foundation (No.BK20130053). We are also grateful to the High Performance Computing Center (HPCC) of Nanjing University for doing the numerical calculations in this paper on its IBM Blade cluster system.

References

1. A. Fujishima, *Nature*, 1972, **238**, 37-38.
2. M. Grätzel, *Nature*, 2001, **414**, 338-344.
3. Z. Li, W. Luo, M. Zhang, J. Feng and Z. Zou, *Energ. Environ. Sci.*, 2013, **6**, 347-370.
4. M. Hara, G. Hitoki, T. Takata, J. N. Kondo, H. Kobayashi and K. Domen, *Catal. Today*, 2003, **78**, 555-560.
5. M. Liao, J. Feng, W. Luo, Z. Wang, J. Zhang, Z. Li, T. Yu and Z. Zou, *Adv. Funct. Mater.*, 2012, **22**, 3066-3074.
6. M. Li, W. Luo, D. Cao, X. Zhao, Z. Li, T. Yu and Z. Zou, *Angew. Chem. Int. Ed.*, 2013, **52**, 11016-11020.
7. A. Murphy, P. Barnes, L. Randeniya, I. Plumb, I. Grey, M. Horne and J. Glasscock, *Int. J. Hydrogen Energy*, 2006, **31**, 1999-2017.
8. M. Ritala, P. Kalsi, D. Riihelä, K. Kukli, M. Leskelä and J. Jokinen, *Chem. Mater.*, 1999, **11**, 1712-1718.
9. S. J. Henderson and A. L. Hector, *J. Solid State Chem.*, 2006, **179**, 3518-3524.
10. E. Watanabe, H. Ushiyama and K. Yamashita, *Chem. Phys. Lett.*, 2013, **561**, 57-62.
11. J. Wang, W. Luo, J. Feng, L. Zhang, Z. Li and Z. Zou, *Phys. Chem. Chem. Phys.*, 2013, **15**, 16054-16064.

12. P. Ravindran, L. Fast, P. Korzhavyi, B. Johansson, J. Wills and O. Eriksson, *J. Appl. Phys.*, 1998, **84**, 4891-4904.
13. R. Hill, *Proc. Phys. Soc.*, 1952, **65**, 349-354.
14. R. Ramprasad, H. Zhu, P. Rinke and M. Scheffler, *Phys. Rev. Lett.*, 2012, **108**, 066404.
15. J. Heyd, G. E. Scuseria and M. Ernzerhof, *J. Chem. Phys.*, 2003, **118**, 8207-8215.
16. J. P. Perdew, K. Burke and M. Ernzerhof, *Phys. Rev. Lett.*, 1996, **77**, 3865-3868.
17. A. V. Krukau, O. A. Vydrov, A. F. Izmaylov and G. E. Scuseria, *J. Chem. Phys.*, 2006, **125**, 224106.
18. C. G. Van de Walle and J. Neugebauer, *J. Appl. Phys.*, 2004, **95**, 3851-3879.
19. G. Kresse and J. Furthmüller, *Phys. Rev. B*, 1996, **54**, 11169.
20. P. E. Blöchl, *Phys. Rev. B*, 1994, **50**, 17953.
21. C. Jiang, Z. Lin and Y. Zhao, *Phys. Rev. Lett.*, 2009, **103**, 185501.
22. A. Friedrich, B. Winkler, L. Bayarjargal, E. A. Juarez Arellano, W. Morgenroth, J. Biehler, F. Schröder, J. Yan and S. M. Clark, *J. Alloys Compd.*, 2010, **502**, 5-12.
23. O. Beckstein, J. Klepeis, G. Hart and O. Pankratov, *Phys. Rev. B*, 2001, **63**, 134112.
24. J. D. Houmes and H.-C. z. Loye, *J. Solid State Chem.*, 1996, **127**, 267-275.
25. S. Hosseini, T. Movlarooy and A. Kompany, *Physica B: Condensed Matter*, 2007, **391**, 316-321.
26. A. Janotti, J. Varley, P. Rinke, N. Umezawa, G. Kresse and C. Van de Walle, *Phys. Rev. B*, 2010, **81**, 085212.
27. S. Ouyang, H. Tong, N. Umezawa, J. Cao, P. Li, Y. Bi, Y. Zhang and J. Ye, *J. Am. Chem. Soc.*, 2012, **134**, 1974-1977.

Table 1. Single-crystal elastic constants c_{ij} (GPa), polycrystalline bulk modulus B (GPa), shear modulus G (GPa), and Young's modulus E (GPa) of the pure Ta_3N_5, $Ta_3N_5+V_N$ and $Ta_3N_5+O_N$.

Structures	c_{11}	c_{22}	c_{33}	c_{44}	c_{55}	c_{66}	c_{12}	c_{13}	c_{23}	B	G	E
pure Ta_3N_5	377	399	396	114	124	58	216	171	128	244	98	260
$Ta_3N_5+V_N$	356	335	330	67	116	52	187	152	119	214	81	215
$Ta_3N_5+O_N$	388	384	395	99	118	58	215	167	132	242	94	251

Figure captions

Fig. 1. (a) Unit cell of the conventional bulk Ta_3N_5. The yellow and grey balls are Ta and N atoms, respectively. (b) *k*-point path (solid red line) in the Brillouin zone (dashed blue line) of the conventional Ta_3N_5 unit cell structure for the band structure calculation. (c) Band structure of the conventional Ta_3N_5. The valence band maximum (VBM) and valence band minimum (VBm) are labeled.

Fig. 2. Correlation between the defects formation energies (upper: $Ta_3N_5+V_N$; lower: $Ta_3N_5+O_N$) and the valence band width (VBW) of the pure Ta_3N_5 calculated by different hybrid functionals.

Fig. 3. (a) and (b) are the valance band width and cohesive energy, respectively, of the pure Ta_3N_5, $Ta_3N_5+V_N$ and $Ta_3N_5+O_N$ calculated by different hybrid functionals.

Fig. 4. Valence bands of the (a) pure Ta_3N_5, (b) $Ta_3N_5+O_N$ and (c) $Ta_3N_5+V_N$. The VBMs are aligned for comparison purpose. The four valence bands with the lowest energy in each case are colored. The VBm at the T point in the pure Ta_3N_5 is four-fold degeneracy, leading to 15 degenerate states at the T point (T_1 to T_{15}). For the visualization purpose, only T_1, T_2, T_3, T_{13}, T_{14} and T_{15} are labeled. (d) and (e) are the charge density difference of the four valence bands with the lowest energy (colored) between the pure Ta_3N_5 and $Ta_3N_5+O_N$, and that between the pure Ta_3N_5 and $Ta_3N_5+V_N$, respectively. The yellow and green densities represent charge accumulation and depletion, respectively (isosurface level = 0.01 electron per $Å^3$).

Fig. 5. Calculated DOS of (a) Ta_3N_5, (b) $Ta_3N_5+V_N$ and (c) $Ta_3N_5+O_N$ at the PBE level. Calculated DOS of (d) Ta_3N_5, (e) $Ta_3N_5+V_N$ and (f) $Ta_3N_5+O_N$ at the HSE level. The vertical dash line in each case is the Fermi level. The horizontal axes of $Ta_3N_5+V_N$ and $Ta_3N_5+O_N$ are aligned with that of the pure Ta_3N_5 by the electrostatic potential calculations. In the DOS calculated at the PBE level (the same for the HSE level), two solid vertical red lines, which correspond to the VBM and CBM of the pure Ta_3N_5, respectively, go across (a), (b) and (c) for the comparison purpose.

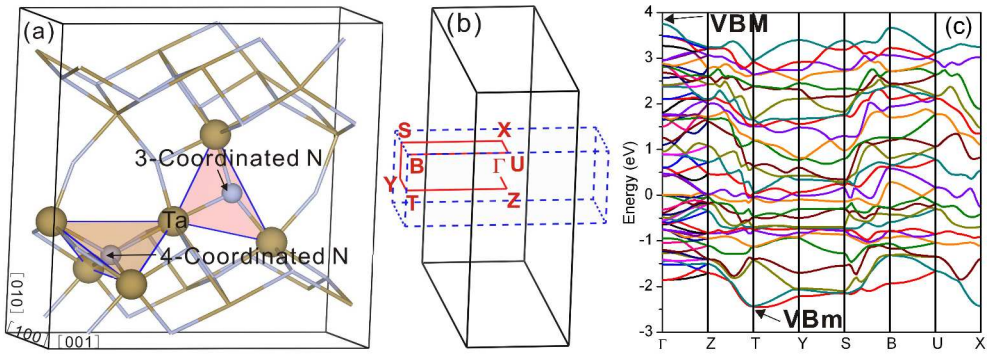

Fig. 1

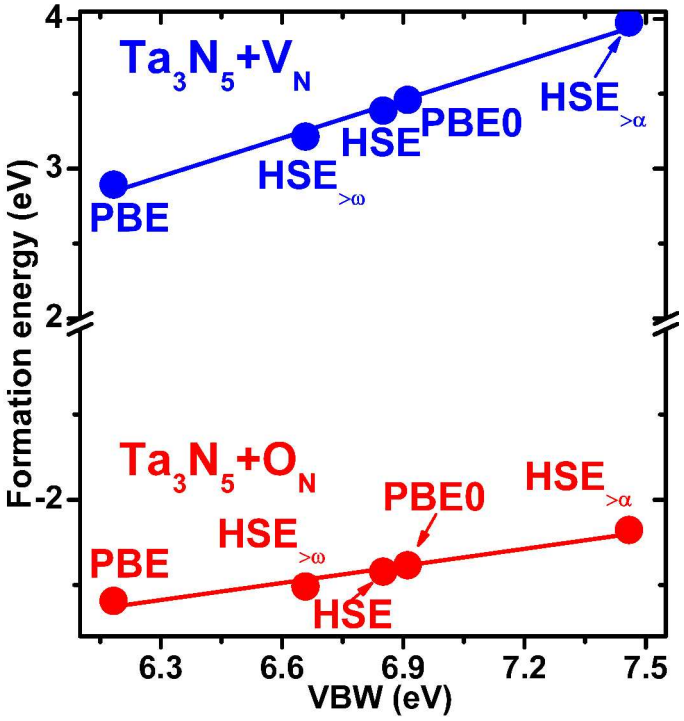

Fig. 2

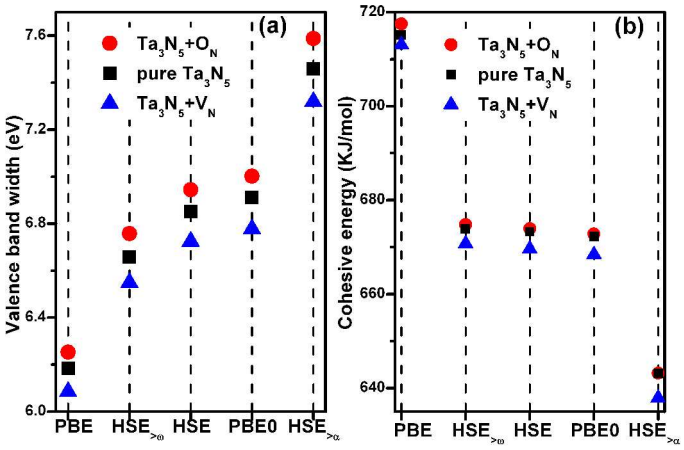

Fig. 3

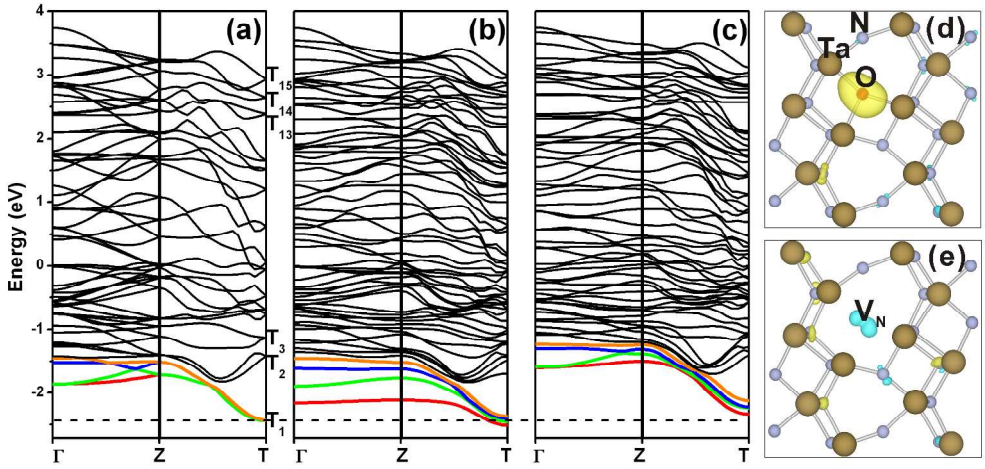

Fig. 4

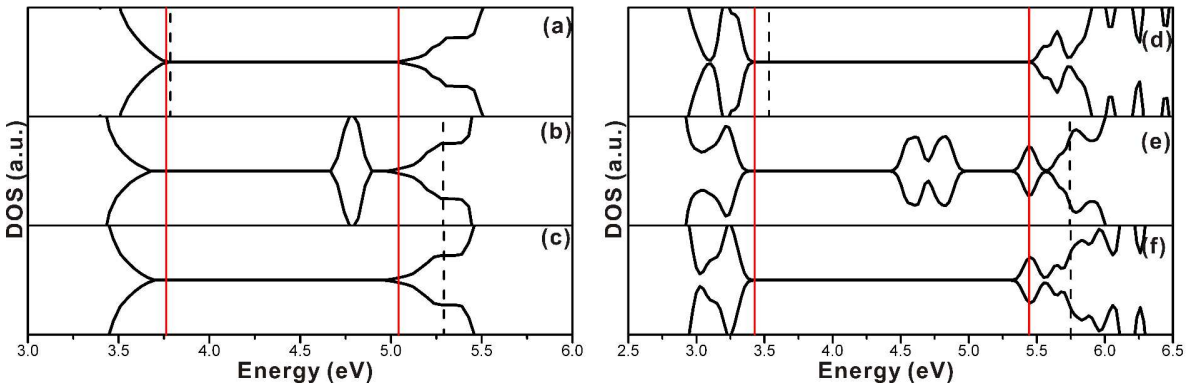

Fig. 5